6

Buckling and Post-Buckling of Parabolic Arches with Local Damage

6.1. Introduction

The birth of fracture mechanics is attributed to Griffith (1920), who based it on the solutions provided by Kirsch (1898) and Inglis (1913). Many efforts to enhance this new branch of solid mechanics followed (Irwin 1957a,b, 1960a,b; Dugdale 1960; Wells 1963; Rice 1968; Rice and Levy 1972). Applications of fracture mechanics to one-dimensional continua were possible after the introduction of the stress intensity factor (SIF) in Irwin (1957a,b). This, together with Castigliano's theorem, allows crack-like damages to be modeled by springs, and the response of beam frames can be described with no need to find the stress field around the crack tip. The structural response includes the displacement profiles due to benchmark load distributions, as well as the frequencies and mode shapes of natural free vibration, which encompass information about geometry, material properties and boundary conditions. A decade before the introduction of SIFs, Kirshmer (1944) and Thomson (1949) focused on simple structures with crack-type damages using a reduced area. Even after the introduction of SIFs, these crack models were used by many researchers.

Dimarogonas (1981, 1982, 1996); Dimarogonas and Paipetis (1983); Anifantis and Dimarogonas (1983a,b,c) successfully used the spring analogy by means of SIFs, especially on rotating machines. These papers paved the way to many more, which focus on building enhanced models for either the crack or the structure and on examining the effects of cracks on the static and dynamic behavior of beam-type structures (Gounaris and Dimarogonas 1988; Ostachowicz and Krawwczuk 1992;

Chapter written by Uğurcan EROĞLU, Giuseppe RUTA, Achille PAOLONE and Ekrem TÜFEKCI.

Modern Trends in Structural and Solid Mechanics 1: Statics and Stability,
First Edition. Edited by Noël Challamel, Julius Kaplunov and Izuru Takewaki.

Chati *et al*. 1997; Khiem and Lien 2001; Sinha and Friswell 2002; Viola *et al*. 2002; Krawczuk *et al*. 2003; Kisa and Arif Gurel 2007; Orhan 2007; Mazanoglu *et al*. 2009; Caddemi and Morassi 2013; Caddemi *et al*. 2017; Caliò *et al*. 2017; Cannizzaro *et al*. 2017; Eroglu and Tufekci 2017b; Eroglu *et al*. 2019, 2020), without pretending to be exhaustive. A thorough investigation of the structural response suggested that monitoring the mechanical behavior of cracked elements may lead to damage identification by suitable methods. Thus, many papers focused on experimental settings, optimization techniques and their effects on identification procedures (Cawley and Adams 1979; Ju and Minovich 1986; Cerri and Ruta 2004; Cerri *et al*. 2008; Pau *et al*. 2010; Ciambella and Vestroni 2015; Capecchi *et al*. 2016; Eroglu and Tufekci 2016, 2017a; Caddemi and Morassi 2007, 2011; Greco and Pau 2011). A survey of the entire literature is out of our scope, yet, we may refer to the review of Doebling *et al*. (1996) for details.

Most studies on cracked one-dimensional structural elements deal with their statics and free dynamics, while their stability is only given marginal consideration, especially arches. A possible reason for this is that stability analysis is usually related to structural design and functioning, and is not meant for structural monitoring purposes. We may quote Karaagac *et al*. (2011), who examined the static and dynamic stability of circular arches by the finite element technique. They used the SIFs provided in Müller *et al*. (1993) and assumed the crack on the inner surface of the arch.

We investigate buckling and post-buckling of parabolic arches with crack-like damages. The latter may be simplified models of either the failure of connections of large structures and actual cracks in relatively small-size applications. We model the arch as a one-dimensional curved beam and study its fundamental and bifurcated path under reasonable kinematic and constitutive assumptions. The crack is modeled by the spring analogy and the SIFs, following literature and previous works by the authors. The novel points here are: a) the fundamental path is non-trivial, in that we linearize the finite field equations and find a non-zero linear elastic response to a uniform load with respect to the arch span; b) the critical values of the load multiplier are found in closed form; c) the germ of the post-buckling path is found by an additional perturbation of the finite field equations about the bifurcation point, providing information on the quality of the bifurcated path. Thorough comments and mechanical interpretations, in light of classic results on stability, are provided, together with hints on possible applications and future developments.

6.2. A one-dimensional model for arches

We model arches as initially curved fully deformable beams, i.e. one-dimensional structured continua that are assumed flexible, extensible and shear-deformable. Then, we suppose that their reference shape is well defined starting from a segment of a

regular planar curve, called the arch axis. The curve segment lies on a plane. On the latter we fix a Cartesian frame x, y, to which a consistent basis of unit vectors $\{\mathbf{e}_x, \mathbf{e}_y\}$ is associated. A third unit vector $\mathbf{e}_z$, which coincides with one of the unit normals to the plane of the arch axis, completes a vector basis for the vector space associated with the three-dimensional Euclidean ambient space. The position of any point P of the axis is described by the vector field $\mathbf{r}_0$

$$\mathbf{r}_0(x) = x\mathbf{e}_x + y(x)\mathbf{e}_y, \quad 0 \le x \le \bar{x},\ y(0) \le y \le y(\bar{x}) \tag{6.1}$$

The tangent vector to the arch axis at any point P and its unit counterpart $\mathbf{l}(s)$ are

$$\begin{aligned} \frac{d\mathbf{r}_0(x)}{dx} = \mathbf{e}_x - \frac{dy(x)}{dx}\mathbf{e}_y, \qquad ds = \sqrt{\frac{d\mathbf{r}_0(x)}{dx} \cdot \frac{d\mathbf{r}_0(x)}{dx}}\,dx, \\ \mathbf{l}(x(s)) = \frac{d\mathbf{r}_0(x(s))}{dx(s)}\frac{dx(s)}{ds}, \end{aligned} \tag{6.2}$$

where ds is the arc length, which is a measure of an element of the axis compatible with the given Cartesian metrics. Equation $[6.2]_2$ yields the intrinsic abscissa s in terms of x and vice versa; hence, $\mathbf{r}_0$ and all the fields depending on P may be expressed in terms of either x or s; thus, equation $[6.2]_3$ gives the field of unit vectors tangent to the axis.

The s-derivative of the field $\mathbf{l}(x(s))$, its magnitude and its unit counterpart are

$$\begin{aligned} \frac{d\mathbf{l}(x(s))}{ds} = \frac{d\mathbf{l}(x(s))}{dx(s)}\frac{dx(s)}{ds} =: k(x(s))\mathbf{m}(x(s)), \\ \mathbf{m}(x(s)) = \frac{1}{k(x(s))}\frac{d\mathbf{l}(x(s))}{ds} \end{aligned} \tag{6.3}$$

The quantity k is the local curvature of the axis at P; the Frénet–Serret local basis consists of the triad $\{\mathbf{l}, \mathbf{m}, \mathbf{n}\}$, $\mathbf{n} = \mathbf{l} \times \mathbf{m}$. Since the axis is a plane curve, the unit tangents and normals depend on P, while the bi-normal does not and coincides, with the exception of the a sign depending on the location of the osculating circle at P, with $\mathbf{e}_z$.

The reference shape is a three-dimensional region that is completed by attaching the copies of a prototype plane figure to any point of the axis. These are called transverse cross-sections and, being all equal, model an arch with uniform geometry with respect to the axis. With no loss in generality, the cross-sections are attached to the axis orthogonally to the unit tangent to the axis. That is, the initial setting of the cross-sections is determined by the Frénet–Serret local triad of unit base vectors for any point of the axis: the arch element is along the unit tangent $\mathbf{l}$, the corresponding cross-section lies in the plane spanned by the unit normal $\mathbf{m}$ and the unit bi-normal $\mathbf{n}$.

For simplicity, the dependence on $x(s)$ will be dropped if no confusion arises.

6.2.1. *Finite kinematics and balance, linear elastic law*

The reference configuration is supposed to be stress-free (i.e. the arch is in an initial natural state). A different shape is provided by the fields $\mathbf{d}$, the vector of the axis displacement (equivalently, by the new position $\mathbf{r} = \mathbf{r}_0 + \mathbf{d}\ \forall P$), and $\mathbf{R}$, the orthogonal tensor of the cross-section's rotation; both are functions of P, hence of x (or s) and of an evolution parameter (time, for instance).

Neutral, or rigid, changes of shape are characterized by a uniform value of $\mathbf{R}$ and by a tangent vector in the new shape that is simply the $\mathbf{R}$-transformed of $\mathbf{l}$. If primes denote s-derivatives to shorten the notation, finite deformation measures in the actual configuration are thus (see Antman (1973, 1995) and Pignataro *et al.* (2008))

$$\mathbf{v} = (\mathbf{r}_0 + \mathbf{d})' - \mathbf{R}\mathbf{l}, \quad \mathbf{V} = \mathbf{R}'\mathbf{R}^\top \qquad [6.4]$$

The components of the vector field $\mathbf{v}$ are the elongation ε of the axis and the shearing strains γ between the axis and the cross-sections; the non-zero components of the skew-symmetric tensor field $\mathbf{V}$ are the variation of curvature χ of the axis.

If we suppose the loads and the change of shape take place in the same plane of the referential configuration, $\mathbf{R}$ is expressed in terms of a single angle ϑ, providing the rotation of the cross-section at P about the bi-normal $\mathbf{n}$, and the displacement field has just two components:

$$(\mathbf{R}) = \begin{pmatrix} \cos\vartheta & -\sin\vartheta \\ \sin\vartheta & \cos\vartheta \end{pmatrix}, \qquad \mathbf{d} = u\mathbf{l} + v\mathbf{m} \qquad [6.5]$$

Then, we have only two and one components of the strain measures $\mathbf{v}, \mathbf{V}$, respectively

$$\varepsilon = 1 - \cos\vartheta + kv + u', \qquad \gamma = -\sin\vartheta + ku + v', \qquad \chi = \vartheta' \qquad [6.6]$$

The environment acts on the arch by: a vector force field, power dual of the incremental displacement of the axis; and a skew-symmetric tensor couple field, power dual of the incremental rotation of the cross-sections. Force and couple may be either distributed (actions at a distance) and localized at the end cross-sections (actions by contact); they are denoted $\mathbf{b}, \mathbf{B}, \mathbf{f}, \mathbf{F}$, respectively. The parts of the arch interact by contact via a vector and a skew symmetric tensor field, power duals of the incremental strains, denoted $\mathbf{t}, \mathbf{T}$, respectively. All the action fields are functions of the place P along the axis and of the evolution parameter, in general.

The balance equations in the configuration at a given value of the evolution parameter, also called actual shape, may be derived either by applying the virtual

work principle or by assuming balance of force and torque as a basic principle. In both cases, they read (see Antman (1973, 1995) and Pignataro *et al.* (2008))

$$\begin{gathered}\mathbf{t}' + \mathbf{b} = \mathbf{0}, \qquad \mathbf{T}' + (\mathbf{r}_0 + \mathbf{d})' \wedge \mathbf{t} + \mathbf{B} = \mathbf{0} \quad \forall x \in (-l, l), \\ \mathbf{t} = \pm \mathbf{t}_{\pm l}, \qquad \mathbf{T} = \pm \mathbf{T}_{\pm l} \quad x = \pm l\end{gathered} \tag{6.7}$$

with $\wedge$ the external product of vectors, providing skew-symmetric tensors. The balance of torque has a parallel expression in terms of axial vectors of skew-symmetric tensors and the cross-product between them. The two components of the inner force and the sole component of the inner couple, with respect to the local basis in the actual configuration, will be denoted $\tilde{N}, \tilde{T}, \tilde{M}$, respectively; they are usually named normal and transverse (or shearing) force and bending couple, respectively.

The components of the inner actions are resultants and resultant moments of Cauchy stresses (i.e., surface densities of contact force in the actual shape). It is customary in structural mechanics, however, to express them in terms of the inner actions in the reference configuration, with components denoted N, T, M, respectively (this is what is usually done by Cauchy and Piola stresses in three-dimensional continuum mechanics). The two sets of components are related via the rotation tensor $\mathbf{R}$ in equation $[6.5]_1$, ruling the change of unit vectors solidal to the cross-sections.

Then, the scalar consequences of equation [6.7] in the presence of planar external actions with components n, t, m, with respect to the local basis in the actual shape, read

$$\begin{aligned}&N' - kT + n = 0, \qquad T' + kN + t = 0, \\ &M' - N(\sin\vartheta + \gamma) + T(\cos\vartheta + \varepsilon) + m = 0\end{aligned} \tag{6.8}$$

Here, the local curvature k appears due to the Frénet–Serret formulas for the s-derivatives of the intrinsic local basis.

Even though kinematics is in a finite setting and balance is written in the actual configuration in terms of the inner actions in the reference shape, we admit that the inner actions are linearly related to the strain measure components by elastic uncoupled constitutive laws, according to

$$\tilde{N} = EA\varepsilon, \qquad \tilde{T} = GA_s\gamma, \qquad \tilde{M} = EI\chi \tag{6.9}$$

where E, G are Young's and transverse elastic moduli of the material of the arch, respectively, and A, A_s, I are the cross-sectional area, shearing area and second moment of area relative to a principal axis of inertia parallel to $\mathbf{n}$, respectively. The positions in equation [6.9] are reasonable in that we will operate a perturbation of the finite field equations, and linear (incremental) constitutive equations suffice to

describe the arch response. The uncoupled laws in equation [6.9], similar to those provided by Saint-Venant's theory, are reasonable enough for compact cross-sections with main dimensions that are small compared with the local radius of the osculating circle (see Timoshenko and Goodier (1951)).

Then, taking into account that the local frame attached to the cross-section changes according to the orthogonal tensor $\mathbf{R}$ in equation [6.5], the constitutive relations in equation [6.9] can be given in terms of the components of the inner action in the reference shape, providing

$$\varepsilon = N\left(\frac{\cos^2\vartheta}{EA} + \frac{\sin^2\vartheta}{GA_s}\right) + T\sin\vartheta\cos\vartheta\left(\frac{1}{EA} - \frac{1}{GA_s}\right),$$
$$\gamma = T\left(\frac{\cos^2\vartheta}{GA_s} + \frac{\sin^2\vartheta}{EA}\right) + N\sin\vartheta\cos\vartheta\left(\frac{1}{EA} - \frac{1}{GA_s}\right),\ \ \chi = \frac{M}{EI} \qquad [6.10]$$

In the following sections, we describe how we use the set of field equations for the arch in order to follow its response to an external load uniformly distributed with respect to the metrics of the span and monotonically increasing. A perturbation approach will follow a linearized solution in the neighborhood of the referential configuration (fundamental path), until a critical value of the load multiplier is reached. This corresponds to a bifurcation of the static equilibrium; in order to follow the jet of the bifurcated path, a second perturbation of the field equations in the neighborhood of the buckled shape will be performed.

6.2.2. *Non-trivial fundamental equilibrium path*

The field equations [6.6], [6.8] and [6.10] form a system of ordinary differential equations with respect to the spatial coordinate of any point P of the arch axis. To find the static response to any set of distributed external actions n, t, m in the actual shape, we are supposed to solve this nonlinear differential system, supplemented by the relevant boundary conditions. Let all external actions be rescaled by a load multiplier: then, the solutions of the field equations provide a one-parameter family of new shapes, called the fundamental path, which is described in exact, nonlinear, finite form. It goes without saying that, bar very special cases, the resolution of the field equations in finite form is computationally very demanding.

However, in structural engineering, we usually do not face finite displacements, and we may assume the structural response to be limited to "small" displacements and rotations. Hence, linearization of the field equations is possible, and the search for the fundamental path is greatly simplified. To this aim, let us introduce an evolution parameter $\eta \in [0, 1]$ such that $\eta = 0$, $\eta = 1$ characterize the reference and the actual shape, respectively. A perturbation approach, i.e., a formal power series expansion

of all the fields of interest in terms of η, provides an approximate response of the structure about a given value of the evolution parameter (see Pignataro *et al.* (1991)). If we thus let $\eta = 0$ and limit the formal expansion at the first order, we study a non-trivial neighborhood of the reference configuration, supposed to represent the natural state of the arch. Then, if the suffix 0 denotes quantities evaluated in the reference shape,

$$\mathbf{R}_0 = \mathbf{I} \Leftrightarrow \vartheta_0 = 0, \qquad \mathbf{d}_0 = \mathbf{0}, \qquad N_0 = T_0 = M_0 = 0 \tag{6.11}$$

Hence, the linear expansion of equations [6.6], [6.8] and [6.10] about the unstressed reference state provides

$$\begin{aligned} &EA(\dot{u}'_f - k\dot{v}_f) = \dot{N}_f, \quad GA_s(\dot{v}'_f - \dot{\vartheta}_f + k\dot{u}_f) = \dot{T}_f, \quad EI\dot{\vartheta}'_f = \dot{M}_f, \\ &\dot{N}'_f - k\dot{T}_f + \dot{n}_f = 0, \quad \dot{T}'_f + k\dot{N}_f + \dot{t}_f = 0, \quad \dot{M}'_f + \dot{T}_f + \dot{m}_f = 0, \end{aligned} \tag{6.12}$$

where the overdot denotes η-derivatives of functions evaluated at $\eta = 0$; the suffix f indicates fields along the fundamental path. As is well known, the fundamental path is a single-valued curve expressing a characteristic displacement (or strain) versus the load multiplier when the latter monotonically grows from zero. When the load multiplier attains a so-called critical value, the equilibrium path becomes a multi-valued curve and bifurcation of the static solution occurs (see Pignataro *et al.* (1991)).

6.2.3. *Bifurcated path*

To investigate the static bifurcation phenomenon in a neighborhood of the critical point, we assume that any function g of interest in this problem may be written in the additive form $g = g_f + g_b$, where the subscripts f and b denote the values of g in the fundamental and bifurcated paths, respectively. If we let $g_b = 0$, we investigate the fundamental path only; if $g_b \neq 0$ and we add it to g_f, we obtain the value attained by g in the bifurcated path when departing from the fundamental one.

Let us investigate a neighborhood of the bifurcation point, found by evaluating the critical value of the load multiplier along the fundamental path. Then, we suppose that any function of interest along the bifurcated path regularly depends on another evolution parameter β, equal to zero at the bifurcation point and growing along the bifurcated path. We may thus perform a power series expansion of g_b in terms of β about the critical point $\beta = 0$ (see Pignataro *et al.* (1991)); if overdots now stand for the β-derivatives evaluated at $\beta = 0$ and $g_b(\beta = 0) = 0$, i.e. $g(\beta = 0) = g_f$, we have

$$g_b = 0 + \beta\dot{g} + (\beta^2/2)\ddot{g} + \dots \tag{6.13}$$

Performing such an expansion for the system of equations [6.6], [6.8] and [6.10], where all functions of interest are now evaluated along the bifurcated path, we obtain

a hierarchy of systems of ordinary differential equations, one at each order of the β-formal power series expansion (see Pignataro *et al.* (1991)).

The first set of the hierarchy provides the first-order germ of the bifurcated path and accounts for the quantities of the fundamental path at the critical point

$$\begin{aligned}
&-k\dot{v}_b + \sin\vartheta_f\dot{\vartheta}_b + \dot{u}_b' = \frac{\dot{N}_b}{EA} + T_f\vartheta_b\left(\frac{1}{EA} - \frac{1}{GA_s}\right) = \dot{\varepsilon}_b,\\
&k\dot{u}_b - \cos\vartheta_f\dot{\vartheta}_b + \dot{v}_b' = \frac{\dot{T}_b}{GA_s} + N_f\vartheta_b\left(\frac{1}{EA} - \frac{1}{GA_s}\right) = \dot{\gamma}_b,\\
&\dot{\vartheta}_b' = \frac{\dot{M}_b}{EI}, \qquad \dot{N}_b' - k\dot{T}_b + \dot{n}_b = 0, \qquad \dot{T}_b' + k\dot{N}_b + \dot{t}_b = 0,\\
&\quad \dot{M}_b' - N_f(\gamma_b + \cos\vartheta_f\dot{\vartheta}_b) - \dot{N}_b(\gamma_f + \sin\vartheta_f) +\\
&\quad + T_f(\dot{\varepsilon}_b - \sin\vartheta_f\dot{\vartheta}_b) + \dot{T}_b(\cos\vartheta_f + \varepsilon_f) + \dot{m}_b = 0
\end{aligned} \tag{6.14}$$

The terms along the fundamental path may be replaced with those evaluated by the η-linearization discussed in the previous section, since we assumed that the fundamental path, however non-trivial, consists of shapes adjacent to the reference configuration. Thus, equation [6.14] becomes

$$\begin{aligned}
&u_b' - kv_b = \frac{N_b}{EA} + T_f\vartheta_b\left(\frac{1}{EA} - \frac{1}{GA_s}\right) - \vartheta_f\vartheta_b\\
&v_b' + ku_b - \vartheta_b = \frac{T_b}{GA_s} + N_f\vartheta_b\left(\frac{1}{EA} - \frac{1}{GA_s}\right),\\
&EI\vartheta_b' = M_b \qquad N_b' - kT_b + n_b = 0, \qquad T_b' + kN_b + t_b = 0,\\
&M_b' - N_f(\gamma_b + \vartheta_b) - N_b(\gamma_f + \vartheta_f) + T_f(\varepsilon_b - \vartheta_f\vartheta_b) + T_b(1 + \varepsilon_f) + m_b = 0
\end{aligned} \tag{6.15}$$

where all overdots are omitted for a simpler notation: all quantities are thus actually first-order increments (with the exception of the curvature k in the reference configuration): those with subscript f are with respect to the reference configuration, and those with subscript b with respect to the critical state. The solution to the set in equation [6.15] provides the first-order bifurcated path with respect to β, accounting for the strains and inner actions attained at the bifurcation point.

Next, we show a couple of meaningful benchmark examples to show how the proposed two-parameter perturbation expansions work and provide known results.

6.2.4. *Special benchmark examples*

Here, we provide qualitative evidence on the generality of the differential system [6.15]. We present two benchmark examples from the literature; since shearing strain is neglected in these, we admit the same inner constraint, without loss of generality.

Straight compressed beams. In a straight ($k = 0$) and slender ($\gamma = 0$) beam subjected only to a compressive force P, it is immediate to see that the non-trivial linear response, describing the fundamental path, is

$$\gamma_f = 0, \quad \varepsilon_f = -P/EA, \quad \vartheta_f = 0, \quad N_f = -P, \quad T_f = M_f = 0 \qquad [6.16]$$

Substituting equation [6.16] into equation [6.15] leads to the set of linear differential equations

$$\begin{aligned} &EAu_b' = N_b, \qquad v_b' = \vartheta_b(1-\varepsilon_f), \qquad EI\vartheta_b' = M_b, \\ &N_b' = T_b' = 0, \qquad M_b' + P\vartheta_b + T_b(1-\varepsilon_f) = 0 \end{aligned} \qquad [6.17]$$

which can be rearranged as

$$EAu_b'' = 0, \qquad EIv_b^{IV} + P\,(1-\varepsilon_f)\,v_b'' = 0 \qquad [6.18]$$

Equations [6.18] are identical to the first two of (31) in Pignataro and Ruta (2003), and we also find them in Pflüger (1964). If we neglect the initial contraction, i.e. $\varepsilon_f = 0$, equations [6.18] coincide with the well-known differential equations for Euler buckling.

Circular arch under radial load. A portion of a slender ($\gamma = 0$) circular arch of radius R has uniform initial curvature $k = 1/R$ and is loaded by a uniform radial distribution of magnitude q with the same direction throughout the motion (i.e. "dead" or conservative). If, as is usual in the literature, the arch is supported by rollers, the only non-zero fields of the fundamental path follow "Mariotte's formula"

$$\varepsilon_f = -(qR)/(EA), \quad N_f = -qR \qquad [6.19]$$

Substituting equation [6.19] into equation [6.15] leads to the set of linear differential equations

$$\begin{aligned} &u_b' - \frac{v_b}{R} = \frac{N_b}{EA}, \qquad v_b' - \vartheta_b\left(1 - \frac{qR}{EA}\right) + \frac{u_b}{R} = 0, \\ &\vartheta_b' = \frac{M_b}{EI}, \qquad N_b' - \frac{T_b}{R} - q\vartheta_b = 0, \\ &T_b' + \frac{N_b}{R} = 0, \qquad M_b' + qR\vartheta_b + T_b\left(1 - \frac{qR}{EA}\right) = 0 \end{aligned} \qquad [6.20]$$

If the axial strain is negligible, i.e. $1 - (qR/EA) \approx 1$, the system [6.20] becomes

$$\begin{aligned} &EA\left(u_b' - \frac{v_b}{R}\right) - qR^2\left(v_b'' + \frac{u_b'}{R}\right) - REI\left(v_b^{IV} + \frac{u_b'''}{R}\right) = 0 \\ &EI\left(v_b''' + \frac{u_b''}{R}\right) + REA\left(u_b'' - \frac{v_b'}{R}\right) - qR\left(v_b' + \frac{u_b}{R}\right) = 0 \end{aligned} \qquad [6.21]$$

Equation [6.21] is identical to those of Simitses and Hodges (2006), after suitably changing the independent variable and the orientation of the radial displacement.

From these two benchmark studies, we deduce that the two-parameter perturbation expansions of the finite field equations proposed here are a reliable tool for investigating the static stability of non-trivial equilibria. In the next section, we investigate parabolic arches, which are the main objectives of our study.

6.3. Parabolic arches

Parabolic arches are curved beams, the axes of which are described by a segment of parabola, symmetric with respect to its vertex. We fix the coordinate frame as in Figure 6.1; thus, the position vector of the points of the axis is

$$\mathbf{r}_0(x) = x\mathbf{e}_x + f[1 - (x^2/l^2)]\mathbf{e}_y, \quad -l \le x \le l,\ 0 \le y \le f \qquad [6.22]$$

in terms of the Cartesian abscissa x along the span, $2l$ long; f is the height of the arch crown with respect to the line of the span, connecting the two ends.

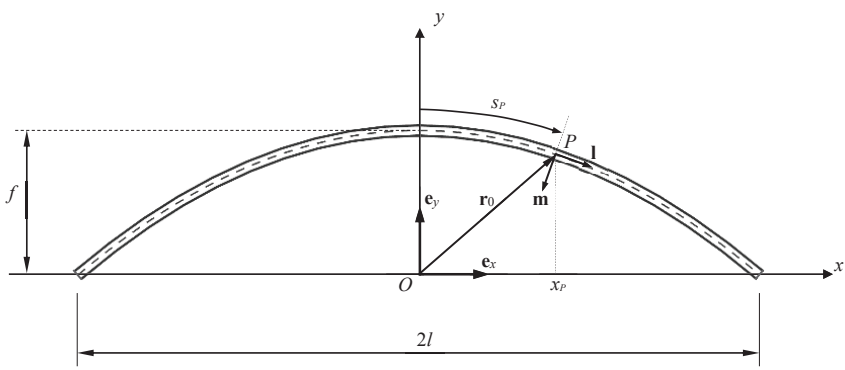

Figure 6.1. *Reference shape of a parabolic arch with cross-sections orthogonal to the axis*

By equations [6.2] and [6.3], the tangent vectors, their magnitude (the arc length), their unit counterpart $\mathbf{l}$, the local curvature and unit normals are

$$\frac{d\mathbf{r}_0}{dx} = \mathbf{e}_x - f\frac{2x}{l^2}\mathbf{e}_y, \quad ds = \sqrt{1 + \frac{4f^2x^2}{l^4}}dx, \quad \mathbf{l} = \frac{l^2\mathbf{e}_x - 2fx\mathbf{e}_y}{\sqrt{l^4 + 4f^2x^2}},$$
$$k = \frac{2fl^4}{(l^4 + 4f^2x^2)^{3/2}}, \qquad \mathbf{m} = -\frac{2fx\mathbf{e}_x + l^2\mathbf{e}_y}{\sqrt{l^4 + 4f^2x^2}} \qquad [6.23]$$

The Frénet–Serret triad in equation [6.23] is completed by the bi-normal $\mathbf{n} = \mathbf{l} \times \mathbf{m} = -\mathbf{e}_z$ (the sign is due to the assigned curvature, with osculating circle below the axis $\forall P$).

To abstract from the particular values of the geometrical and physical quantities in a problem, it is customary to operate non-dimensional analyses; let us then define

$$\begin{aligned}(\bar{x}, \bar{s}, \bar{u}, \bar{v}) &= \frac{(x, s, u, v)}{l}, \quad \alpha = \frac{f}{l}, \quad \lambda = l\sqrt{\frac{A}{I}}, \quad \bar{A} = \frac{GA_s}{EA}, \\ (\bar{N}, \bar{T}) &= \frac{(N, T)l^2}{EI}, \quad \bar{M} = \frac{Ml}{EI}, \quad (\bar{n}, \bar{t}) = \frac{(n, t)l^3}{EI}, \quad \bar{m} = \frac{ml^2}{EI}\end{aligned} \tag{6.24}$$

Equation $[6.23]_2$ provides (at least locally) the functions $x(s)$ and $s(x)$; thus, we may also deduce that $\bar{x} = \bar{x}(\bar{s})$ and equation [6.24] provides further non-dimensional quantities

$$\frac{ds}{dx} = \frac{d\bar{s}}{d\bar{x}} = L(\bar{x}) = \sqrt{1 + 4\alpha^2\bar{x}^2}, \qquad \bar{k}(\bar{x}) = kl = \frac{2\alpha}{L^3(\bar{x})}. \tag{6.25}$$

Substituting equations [6.24] and [6.25] into equation [6.12], the equations for the non-dimensional η-first-order fundamental path are written in matrix form

$$\begin{gathered}\frac{d\mathbf{y}_f}{d\bar{x}} = \mathbf{A}_f\mathbf{y}_f + \mathbf{q}_f, \qquad \mathbf{y}_f = \left\{\bar{u}_f\ \bar{v}_f\ \vartheta_f\ \bar{N}_f\ \bar{T}_f\ \bar{M}_f\right\}^T, \\ \mathbf{q}_f = -L\{0\,0\,0\,\bar{n}_f\ \bar{t}_f\ \bar{m}_f\}^T, \qquad \mathbf{A}_f = L\begin{pmatrix} 0 & k & 0 & \dfrac{1}{\lambda^2} & 0 & 0 \\ -k & 0 & 1 & 0 & \dfrac{1}{\bar{A}\lambda^2} & 0 \\ 0 & 0 & 0 & 0 & 0 & 1 \\ 0 & 0 & 0 & 0 & k & 0 \\ 0 & 0 & 0 & -k & 0 & 0 \\ 0 & 0 & 0 & 0 & -1 & 0 \end{pmatrix}.\end{gathered} \tag{6.26}$$

A force load $-q\mathbf{e}_y$ that is uniform with respect to the span length implies that $m_f = 0 \Rightarrow \bar{m}_f = 0$; its components with respect to the arc length in the local basis are given by the force equivalence

$$-q\mathbf{e}_y\, dx = (n\mathbf{l} + t\mathbf{m})ds \tag{6.27}$$

whence their non-dimensional counterparts according to equations [6.24].

The solution of equation [6.26] is (Hubbard and West 1995; Tufekci *et al.* 2017)

$$\mathbf{y}_f(\bar{x}) = \mathbf{Y}_f(\bar{x})\left[\mathbf{y}_f(\bar{x}_0) + \int_0^{\bar{x}} \mathbf{Y}_f^{-1}(\xi)\,\mathbf{q}(\xi)\,d\xi\right] \tag{6.28}$$

where $\mathbf{Y}(\bar{x})$ is called the principal matrix, or *matricant* (Pease 1965), or *transfer matrix* (Pestel and Leckie 1963), of the homogeneous equation [6.26] about $\bar{x} = 0$. The entries of the principal matrix for a planar curved beam in integral form can be found in Tufekci and Arpaci (2006). They are provided in Eroglu *et al.* (2020) for parabolic arches of uniform cross-sections; variable cross-sections are considered in Eroglu and Ruta (2020). The state vector $\mathbf{y}$ in equation [6.28] accounts for distributed external loads; concentrated ones at any point $\bar{x}_i \in [-1, 1]$ were recently discussed in Eroglu *et al.* (2020) through continuity of displacement and local balance of actions.

We admit that the given load is "dead"; then, it is easy to prove that $n_b = -t_f \vartheta_b, t_b = n_f \vartheta_b$. Substituting equations [6.24] and [6.25] into equations [6.15] provides the equations for the non-dimensional β-first-order bifurcated path in matrix form

$$\frac{d\mathbf{y}_b}{d\bar{x}} = \mathbf{A}_b \mathbf{y}_b\,, \qquad \mathbf{y}_b = \left\{\bar{u}_b\ \bar{v}_b\ \vartheta_b\ \bar{N}_b\ \bar{T}_b\ \bar{M}_b\right\}^T$$

$$\mathbf{A}_b = L \begin{pmatrix} 0 & k & -\vartheta_f + T_f\left(\dfrac{1}{\lambda^2} - \dfrac{1}{\bar{A}\lambda^2}\right) & \dfrac{1}{\lambda^2} & 0 & 0 \\ -k & 0 & 1 + N_f\left(\dfrac{1}{\lambda^2} - \dfrac{1}{\bar{A}\lambda^2}\right) & 0 & \dfrac{1}{\bar{A}\lambda^2} & 0 \\ 0 & 0 & 0 & 0 & 0 & 1 \\ 0 & 0 & t_f & 0 & k & 0 \\ 0 & 0 & -n_f & -k & 0 & 0 \\ 0 & 0 & N_f & \dfrac{T_f}{\bar{A}\lambda^2} + \vartheta_f & -1 - \dfrac{N_f}{\bar{A}\lambda^2} & 0 \end{pmatrix} \qquad [6.29]$$

In a homogeneous arch, the mass per unit length and the bending stiffness are uniform, but the terms in equation [6.29] depend on $\bar{x}$, and $\mathbf{A}_b$ cannot be reduced to an upper triangular form. Hence, equation [6.29], in general, does not have closed-form solutions. Thus, Eroglu *et al.* (2019) propose to find approximate solutions by the Peano series (Peano 1888) and Volterra's multiplicative integral (Pease 1965; Slavik 2007)

$$\begin{aligned} \mathbf{y}_b(\bar{x}) &= \mathbf{Y}_b(\bar{x}, \bar{x}_0)\mathbf{y}_b(\bar{x}_0) \\ \mathbf{Y}_b(\bar{x}, \bar{x}_0) &= \prod_{\imath=1}^{n} \mathbf{Y}_2(\bar{x}_0 + \imath\Delta\bar{x}, \bar{x}_0 + (\imath-1)\Delta\bar{x}), \\ \mathbf{Y}_2(\bar{x}_2, \bar{x}_1) &\approx \mathbf{I} + \mathbf{A}_b(\bar{x}_1)(\bar{x}_2 - \bar{x}_1) + \\ &+ \left(\frac{1}{2}\left.\frac{d\mathbf{A}_b}{dx}\right|_{\bar{x}_1} + \frac{1}{4}\left.\frac{d^2\mathbf{A}_b}{dx^2}\right|_{\bar{x}_1} + \frac{1}{2}\mathbf{A}_b^2(\bar{x}_1)\right)(\bar{x}_2 - \bar{x}_1)^2 \end{aligned} \qquad [6.30]$$

having split $\{\bar{x}, \bar{x}_0\}$ in n intervals with $\Delta\bar{x} = (\bar{x} - \bar{x}_0)/n$. As n increases, $\Delta\bar{x} \to 0$ and equation [6.30] turns into Volterra's integral (Slavik 2007). We keep n finite, yet large enough to ensure convergence.

Equation $[6.30]_1$ requires a point $\bar{x}_0$ where the values of the displacements and contact actions are known. This occurs at the boundary, where non-dimensional natural conditions are (see equation [6.24]):

$$\begin{aligned} \text{clamped end}: &\ \bar{u}=0, \quad \bar{v}=0, \quad \vartheta=0, \\ \text{pinned end}: &\ \bar{u}=0, \quad \bar{v}=0, \quad \bar{M}=0, \\ \text{free end}: &\ \bar{N}=0, \quad \bar{T}=0, \quad \bar{M}=0. \end{aligned} \tag{6.31}$$

They are three such natural conditions at each end, yielding six linear equations in the six components $\mathbf{y}_b$

$$\mathbf{T}(q)\,\mathbf{y}_b(\bar{x}_0)=\mathbf{0} \tag{6.32}$$

with $\mathbf{T}(q)$ a square 6×6 matrix of coefficients. Non-trivial solutions $\mathbf{y}_b(\bar{x}_0)$ require the singularity of $\mathbf{T}(q)$ in terms of the load multiplier q, yielding a highly nonlinear equation, the solutions of which are the critical loads for the arch,

$$\det[\mathbf{T}(q)]=0 \Rightarrow q=q_{cr} \tag{6.33}$$

6.4. Crack models for one-dimensional elements

If the arch has a small plane crack on the cross-section at $\bar{x}_c$, its damaging effect is described by considering two regular arch chunks connected at x_c by a set of springs; as in Eroglu and Tufekci (2017a), their compliances are related to the depth of the crack through its strain energy U_c, given by Tada *et al.* (2000)

$$U_c=\int_{A_c}\frac{1}{E'}\left[\left(\sum K_{I\jmath}\right)^2+\left(\sum K_{II\jmath}\right)^2\right]dA, \quad c_{\imath\jmath}=\frac{\partial^2 U_c}{\partial\imath\partial\jmath}, \imath,\jmath=N,T,M \tag{6.34}$$

where A_c is the cross-section as reduced by the crack; $E'=E/(1-\nu^2)$, with ν Poisson's ratio of the material; $K_{I\jmath}, K_{II\jmath}$ are the stress intensity factors in opening and shearing modes, respectively, due to the $\jmath$-th contact action; and $c_{\imath\jmath}$ is the compliance of the spring representing the effect of the crack on the $\jmath$-th contact action due to a unit value of the $\imath$-th kinematic descriptor.

In a rectangular cross-section of height h with a crack of depth a at opposite sides, with respect to the center of curvature, consider the additional non-dimensional quantities related to the crack

$$\begin{aligned} &\bar{a}=\frac{a}{h}, \quad \bar{K}_{\imath\jmath}=\frac{K_{\imath\jmath}}{E\sqrt{h}}, \quad \bar{U}_c=\frac{U_c}{hEA}, \quad \bar{c}_{\bar{N}\bar{N}}=\frac{EI}{l^3}c_{NN}, \\ &\bar{c}_{\bar{T}\bar{T}}=\frac{EI}{l^3}c_{TT}, \quad \bar{c}_{\bar{M}\bar{M}}=\frac{EI}{l}c_{MM}, \quad \bar{c}_{\bar{M}\bar{N}}=\bar{c}_{\bar{N}\bar{M}}=\frac{EI}{l^2}c_{MN} \end{aligned} \tag{6.35}$$

Following Tada *et al.* (2000), the shape functions f_i of the crack magnitude ratio

$$f_1(\bar{a}) = \sqrt{\frac{2\tan(\pi\bar{a}/2)}{\pi\bar{a}}}\,\frac{0.752+2.02\bar{a}+0.37[1-\sin(\pi\bar{a}/2)]^3}{\cos}(\pi\bar{a}/2),$$

$$f_2(\bar{a}) = \frac{1.22-0.561\bar{a}+0.085\bar{a}^2+0.18\bar{a}^3}{\sqrt{1-\bar{a}}},$$

$$f_3(\bar{a}) = \sqrt{\frac{2\tan(\pi\bar{a}/2)}{\pi\bar{a}}}\,\frac{0.923+0.199\left[1-\sin\left(\pi\bar{a}/2\right)\right]^4}{\cos\left(\pi\bar{a}/2\right)} \qquad [6.36]$$

and equation [6.34] yield the non-dimensional compliances

$$\bar{c}_{\bar{N}\bar{N}} = 4\pi\sqrt{3}(1-\nu^2)\int_0^{\bar{a}}\frac{\xi}{\lambda^3}f_1^2(\xi)\,d\xi,$$

$$\bar{c}_{\bar{T}\bar{T}} = 16\pi\sqrt{3}\frac{1-\nu}{1+\nu}\int_0^{\bar{a}}\frac{\xi}{\bar{A}^2\lambda^3}f_2^2(\xi)d\xi,$$

$$\bar{c}_{\bar{M}\bar{M}} = 12\pi\sqrt{3}(1-\nu^2)\int_0^{\bar{a}}\frac{\xi}{\lambda}f_3^2(\xi)\,d\xi, \qquad [6.37]$$

$$\bar{c}_{\bar{N}\bar{M}} = 12\pi(1-\nu^2)\int_0^{\bar{a}}\frac{\xi}{\lambda^2}f_1(\xi)\,f_3(\xi)\,d\xi.$$

Henceforth, only non-dimensional quantities will be used; with another abuse of notation, overbars will be omitted for simplicity, except when confusion may arise.

The crack at x_c implies a jump of the axis displacement in the actual shape; the jump depends on the contact actions at the cross-sections of the left and right chunks of the arch (whence the superscripts l, r) facing each other at x_c. The inner contact actions at the ends of the fictitious springs will, of course, be balanced. These vector conditions are written in the local basis of the left chunk, pulled by the operator $\mathbf{R}$:

$$\mathbf{R}(\vartheta_r-\vartheta_l)\,\tilde{\mathbf{d}}^r-\tilde{\mathbf{d}}^l=\mathbf{C}^*\tilde{\mathbf{f}}^l, \qquad \mathbf{R}(\vartheta_r-\vartheta_l)\,\tilde{\mathbf{f}}^r=\tilde{\mathbf{f}}^l \qquad [6.38]$$

$$\mathbf{C}^*=\begin{pmatrix} c_{NN} & 0 & pc_{NM} \\ 0 & c_{TT} & 0 \\ pc_{NM} & 0 & c_{MM}\end{pmatrix}$$

The tilde here denotes vectors in actual configuration. For easier calculations, inner actions $\mathbf{f}=\{N,T,M\}^T$ and displacement are written with respect to their components in the reference frame; hence, equation [6.38] becomes

$$\begin{aligned}\mathbf{R}(\vartheta_r-\vartheta_l)\mathbf{R}^T(\vartheta_r)\mathbf{d}^r-\mathbf{R}^T(\vartheta_l)\mathbf{d}^l&=\mathbf{C}^*\mathbf{R}^T(\vartheta_l)\mathbf{f}^l,\\ \mathbf{R}(\vartheta_r-\vartheta_l)\mathbf{R}^T(\vartheta_r)\mathbf{f}^r&=\mathbf{R}^T(\vartheta_l)\mathbf{f}^l\end{aligned} \qquad [6.39]$$

Since $\mathbf{R}\left(\vartheta_r - \vartheta_l\right)\mathbf{R}^T\left(\vartheta_r\right) = \mathbf{R}^T\left(\vartheta_l\right)$, equation [6.39] may be written in matrix form

$$\begin{aligned} \mathbf{y}^r(x_c) &= \mathbf{C}(a,p)\mathbf{y}^l(x_c), \\ \mathbf{C}\left(a,p\right) &= \begin{pmatrix} \mathbf{I} & \mathbf{R}\left(\vartheta_l(x_c)\right)\mathbf{C}^*\mathbf{R}^T\left(\vartheta_l(x_c)\right) \\ \mathbf{0} & \mathbf{I} \end{pmatrix}, \end{aligned} \tag{6.40}$$

where $\mathbf{0}, \mathbf{I}$ are the 3×3 null and identity matrices, respectively, and $p = \pm 1$ is a non-material parameter indicating that the crack is at the top or bottom of the cross-section with respect to the center of curvature, respectively. Equation [6.40] is nonlinear and can be subjected to the same perturbation performed for field equations. When it is linearized about the initial unstressed configuration, the condition $\mathbf{y}^r(x_c) = \mathbf{C}_f\mathbf{y}^l(x_c)$, identical to that in Eroglu *et al.* (2020), is recovered. A linearization about the non-trivial fundamental path leads to the matrix $\mathbf{C}$ depending on ϑ_b, rearranged as

$$\mathbf{y}^r(x_c) = \mathbf{C}_b\mathbf{y}^l(x_c) \tag{6.41}$$

where $\mathbf{C}_b$ is too long to be reported and will be omitted for the sake of space.

For both right and left chunks, equation [6.28], solution for the static problem, holds; the unknown initial values are now 12, and adding the jump to the boundary conditions yields 12 equations for calculating them. It is then better to present the jump conditions in terms of these initial values; if $\hat{\mathbf{I}}$ is the 6×6 identity, equation [6.40] becomes

$$\mathbf{y}_f^r(x_0) = \mathbf{Y}_f^{-1}(x_c)\left(\mathbf{C}_f\mathbf{Y}_f(x_c)\mathbf{y}_f^l(x_0) + \left(\mathbf{C}_f - \hat{\mathbf{I}}\right)\int_0^{x_c}\mathbf{Y}_f^{-1}(\xi)\,\mathbf{q}\left(\xi\right)d\xi\right) \tag{6.42}$$

For the eigenvalue problem equation [6.33] we will then update the principal matrix for a given crack location x_c inside the $\jmath$-th interval between x_0 and x as follows:

$$\begin{aligned} \mathbf{Y}_b(x,x_0) &= \mathbf{Y}_b\left(x, x_0 + \jmath\Delta x\right)\mathbf{Y}_{bc}\mathbf{Y}_b\left(x_0 + \left(\jmath - 1\right)\Delta x, x_0\right) \\ \mathbf{Y}_{bc} &= \mathbf{Y}_2\left(x_0 + \jmath\Delta x, x_c\right)\mathbf{C}_b\mathbf{Y}_2\left(x_c, x_0 + \left(\jmath - 1\right)\Delta x\right) \end{aligned} \tag{6.43}$$

6.5. An application

Consider a fixed parabolic arch with geometric aspect $\alpha = 0.4$ and slenderness ratio $\varsigma = 100$, under the described load; if the cross-section is rectangular, $\bar{A} = 0.3$. The arch is assumed to have a transverse crack at $x = x_c$ with depth ratio $a = 0.6$

(recall that, to simplify the notation, we dropped the overbars for the non-dimensional quantities related to the crack). We refer to Eroglu *et al.* (2020) for a detailed examination of the static problem providing the first-order strain increments, which are assumed to be a sufficiently accurate representation of the actual deformed shape.

If the crack is not at the crown, one of the arch chunks is more "slender" than the other. Then, it is possible that when the former buckles, the latter goes on along its fundamental path; thus, two different principal matrices should be used. In general, both chunks buckle in correspondence to the same load multiplier; in any case, we consider two different scenarios: both chunks bifurcate for the same load multiplier ("global buckling"), or the more slender reaches bifurcation, while the other remains on its fundamental path ("local buckling"). However, recall that the two sub-arches are linked by relatively stiff springs, not by a smooth hinge; i.e. the crack affects a very small portion of the cross-section and does not actually cut the arch in two.

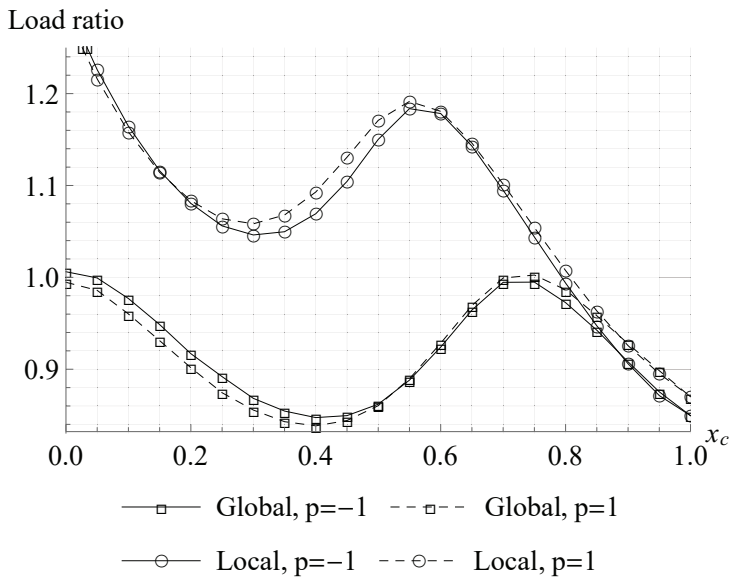

Figure 6.2. *Critical load ratio for a fixed arch with a crack characterized by* $a = 0.6$

Figure 6.2 presents the plot of the critical load ratio (critical load of the cracked arch divided by that of the intact arch) for an arch damaged by a crack with aspect ratio $a = 0.6$ versus the crack location x_c. The plot considers one half of the arch,

because of symmetry, i.e. we plot what happens when the crack is located at the right half of the considered arch. We present the results for both "global" (square markers) and "local" buckling (round markers) and for both crack locations at the opposite sides of the cross-section with respect to the center of curvature (i.e. for the non-material parameter $p = 1$ (full lines) and $p = -1$ (dashed lines)).

We see that "local" buckling requires a greater critical load than the "global" one, except for $x_c \gtrapprox 0.8$, i.e. in the vicinity of the right constraint. This has a clear physical interpretation: when the crack is near the fixed end, the difference in slenderness of the two sub-arches reaches its top; thus, the more slender chunk attains buckling before the more stubby sub-arch. The critical load ratio of this "local" buckling is very high at the beginning, then decreases as x_c approaches the constrained end, resembling that of "global" buckling. This also has a physical interpretation, since for $x_c \approx 0.8$, the stubby chunk actually acts as an extended clamp, then makes the system globally stiffer; on the other hand, when $x_c \to 1$, the system is practically equivalent to the entire arch.

Actually, for other values of x_c, the global buckling prevails, which is also physically reasonable: if both chunks have comparable slenderness, they are similarly prone to buckling and bifurcate as one. We also remark that the effect of the crack position on opposite sides of the cross-section has limited effect on critical load, due to considerations similar to those provided in Eroglu *et al.* (2019). For more shallow arches, we may expect a stronger dependence of the critical load on p.

We remark that at $x_c \approx 0$ and $x_c \approx 0.75$, the critical load ratio attains values greater than unity, i.e. the critical load multiplier of the damaged arch is greater than that of the intact one. This is a seemingly paradoxical behavior, since it was highlighted by Timoshenko and Gere (1961) that a parabolic arch with one hinge at the crown, in general, buckles under a lower critical load with respect to an entire fixed arch. However, we may check that this phenomenon occurs for cracks located at places around which the incremental bending moment vanishes. Therefore, the coupling between axial force and bending moment (accounted for by the parameter p) creates a bending moment, which acts against the buckling strain, providing a stiffening effect. Note that for the problems considered herein, the mode shape is still skew-symmetric, albeit the crack induces some slight deviations from it (see Figure 6.3).

Figure 6.3 shows the buckling modes about the non-trivial fundamental path. The deformed configuration is plotted with an amplification factor of 10, to better reflect the effect of crack location on the section. Effects of crack position on the bifurcated paths are clearly shown; moreover, the question is raised about the stability of bifurcated paths and its dependence on the crack location on the section, which needs to be investigated in future contributions.

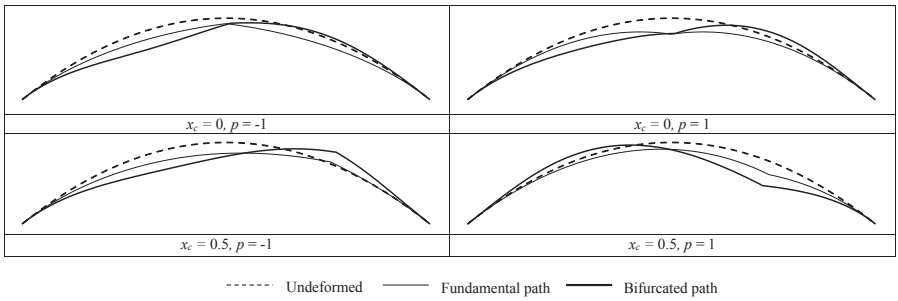

Figure 6.3. *Buckling modes about the deformed shape for* $a = 0.6$

6.5.1. *A comparison*

For comparison, we consider a symmetric circular arch, consisting of two regular identical chunks connected with a torsional spring with stiffness k_T, as in Wang *et al.* (2005). This shape approximates that of a parabolic arch when its opening angle is moderate. The arch has radius R and opening angle φ. This is a primitive model of possible damage at the apex, neglecting axial, and shear compliances as well as axial-bending coupling. For this simplified model, in our treatment, we have a single non-zero component in the compliance matrix, c_{MM}, which equals $1/k_T$.

φ	$\pi/6$	$\pi/6$	$\pi/3$	$\pi/3$	$\pi/2$	$\pi/2$	$2\pi/3$	$2\pi/3$
$\frac{k_T R}{EI}$	W	Present	W	Present	W	Present	W	Present
0	108.36*	108.21*	27.077*	27.052*	12.025*	12.008*	6.7578*	6.755*
2	129.48*	129.30*	36.794	36.737	17.956	17.926	10.806	10.788
4	147.61	147.40	43.979	43.909	21.751	21.712	13.060	13.035
6	163.21	162.97	49.366	49.282	24.277	24.231	14.418	14.388

Table 6.1. *Critical loads for the symmetric mode shapes of a hinged circular arch with a weakened section at the apex. Stars denote that the symmetric mode has a lower critical load than the corresponding skew-symmetric mode; W=Wang* et al. *(2005)*

In the exact treatment in Wang *et al.* (2005), the arch is assumed to be inextensible and shear rigid. Table 6.1 lists the critical loads for symmetric mode shapes: indeed, note that for skew-symmetric mode shape, the bending couple at the apex vanishes and the torsion spring does not affect the behavior. The weakened section only affects the critical load for symmetric mode shapes.

6.6. Final remarks

We presented two perturbation expansions of the finite governing equations for arches modeled as curved beams, in order to investigate their non-trivial fundamental

path and their post-buckling path. Kinematics is finite, balance is in the actual configuration and only constitutive equations are supposed linear elastic. The perturbation approach lets us investigate the effect of a deformed and pre-stressed shape on the buckling load and the relevant equilibria following possible static bifurcation. We showed that this approach recovers well-known benchmark results and applied it to the analysis of buckling scenarios of parabolic arches under a "vertical" load uniformly distributed with respect to the span, affected by small cracks. The effect of the latter is suitably modeled as a set of linear elastic springs, following previous investigations; the solution of the governing equations was found numerically by using the so-called principal matrix of the differential system. We obtained results for both "local" and "global" buckling and commented on them, highlighting how seemingly paradoxical results actually have a clear physical interpretation. Future investigations will be about the quality of the post-buckling path and on linear vibration about non-trivial pre-stressed states, in order to detect the effect of local damages for monitoring purposes.

6.7. Acknowledgments

This work began when Uğurcan Eroğlu was a visiting research student at the Dipartimento di Ingegneria Strutturale e Geotecnica of the Sapienza University of Rome, the support of which is gratefully acknowledged. Giuseppe Ruta acknowledges the support of institutional grants from Sapienza University of Rome for the year 2019.

6.8. References

Anifantis, N. and Dimarogonas, A.D. (1983a). Buckling of rings and tubes with longitudinal cracks. *Mechanics Research Communications*, 18, 693–702.

Anifantis, N. and Dimarogonas, A.D. (1983b). Post buckling behavior of transverse cracked columns. *Composite Structures*, 12(2), 351–356.

Anifantis, N. and Dimarogonas, A.D. (1983c). Stability of columns with a single crack subjected to follower and vertical loads. *International Journal of Solids and Structures*, 19, 281–291.

Antman, S. (1973). *The Theory of Rods*. Springer, Berlin.

Antman, S. (1995). *Nonlinear Problems of Elasticity*. Springer-Verlag, New York.

Caddemi, S. and Morassi, A. (2007). Crack detection in elastic beams by static measurements. *International Journal of Solids and Structures*, 44, 5301–5315.

Caddemi, S. and Morassi, A. (2011). Detecting multiple open cracks in elastic beams by static tests. *Journal of Engineering Mechanics*, 137, 113–124.

Caddemi, S. and Morassi, A. (2013). Multi-cracked Euler–Bernoulli beams: Mathematical modeling and exact solutions. *International Journal of Solids and Structures*, 50, 944–956.

Caddemi, S., Caliò, I., Cannizzaro, F. (2017). The dynamic stiffness matrix (DSM) of axially loaded multi-cracked frames. *Mechanics Research Communications*, 84, 90–97.

Caliò, I., D'Urso, D., Greco, A. (2017). The influence of damage on the eigen-properties of Timoshenko spatial arches. *Computers and Structures*, 190, 13–24.

Cannizzaro, F., Greco, A., Caddemi, S., Caliò, I. (2017). Closed form solutions of a multi-carcked circular arch under static loads. *International Journal of Solids and Structures*, 121, 191–200.

Capecchi, D., Ciambella, J., Pau, A., Vestroni, F. (2016). Damage identification in a parabolic arch by means of natural frequencies, modal shapes and curvatures. *Meccanica*, 51, 2847–2859.

Cawley, P. and Adams, R. (1979). The location of defects in structures from measurements of natural frequencies. *Journal of Strain Analysis*, 14(2), 49–57.

Cerri, M. and Ruta, G. (2004). Detection of localised damage in plane circular arches by frequency data. *Journal of Sound and Vibration*, 270, 39–59.

Cerri, M., Dilena, M., Ruta, G. (2008). Vibration and damage detection in undamaged and cracked circular arches: Experimental and analytical results. *Journal of Sound and Vibration*, 314, 83–94.

Chati, M., Rand, R., Mukherjee, S. (1997). Modal analysis of a cracked beam. *Journal of Sound and Vibration*, 207(2), 249–270.

Ciambella, J. and Vestroni, F. (2015). The use of modal curvatures for damage localization in beam-type structures. *Journal of Sound and Vibration*, 340, 126–137.

Dimarogonas, A.D. (1981). Buckling of rings and tubes with longitudinal cracks. *Mechanics Research Communications*, 8, 179–186.

Dimarogonas, A.D. (1982). Crack identification in aircraft structures. *Proceedings of the First National Aircraft Conference*, pp. 11–22.

Dimarogonas, A.D. (1996). Vibration of cracked structures: A state of the art review. *Engineering Fracture Mechanics*, 55(5), 831–857.

Dimarogonas, A.D. and Paipetis, S. (1983). *Analytical Methods in Rotor Dynamics*. Applied Science, Paris.

Doebling, S., Farrar, C., Prime, M., Shevitz, D. (1996). Damage identification and health monitoring of structural and mechanical systems from changes in their vibration characteristics: A literature review. *Los Alamos Nat. Lab.* Report, LA-13070-MS, pp. 1–129.

Dugdale, D. (1960). Yielding of steel sheets containing slits. *Journal of Mechanical Physics and Solids*, 8, 100–104.

Eroglu, U. and Ruta, G. (2020). Closed-form solutions for elastic tapered parabolic arches under uniform thermal gradients. *Meccanica*, 55, 1135–1152.

Eroglu, U. and Tufekci, E. (2016). Exact solution based finite element formulation of cracked beams for crack detection. *International Journal of Solids and Structures*, 96, 240–253.

Eroglu, U. and Tufekci, E. (2017a). Crack modeling and identification in curved beams using differential evolution. *International Journal of Mechanical Sciences*, 131–132, 435–450.

Eroglu, U. and Tufekci, E. (2017b). Free vibration of damaged frame structures considering the effects of axial extension, shear deformation and rotatory inertia: Exact solution. *International Journal of Structural Stability and Dynamics*, 17(10), 1750111.

Eroglu, U., Ruta, G., Tufekci, E. (2019). Natural frequencies of parabolic arches with a single crack on opposite cross-section sides. *Journal of Vibration and Control*, 25(7), 1313–1325.

Eroglu, U., Paolone, A., Ruta, G., Tufekci, E. (2020). Exact closed-form static solutions for parabolic arches with concentrated damage. *Archive of Applied Mechanics*, 90, 673–689.

Gounaris, G. and Dimarogonas, A. (1988). A finite element of a cracked prismatic beam for structural analysis. *Computers and Structures*, 28(3), 309–313.

Greco, A. and Pau, A. (2011). Detection of a concentrated damage in a parabolic arch by measured static displacements. *Structural Engineering and Mechanics*, 39(6), 751–765.

Griffith, A. (1920). The phenomena of rapture and flow in solids. *Philosophical Transactions of the Royal Society of London*, *Series A*, 221(582–593), 163–198.

Hubbard, J. and West, B. (1995). *Differential Equations: A Dynamical Systems Approach*. Springer-Verlag, New York.

Inglis, C. (1913). Stresses in plates due to the presence of cracks and sharp corners. *Transactions of the Institute of Naval Architects*, 55, 219–241.

Irwin, G. (1957a). Analysis of stresses and strains near the end of a crack traversing a plate. *Journal of Applied Mechanics*, 24, 361–364.

Irwin, G. (1957b). Relation of stresses near a crack to the crack extension force. *Proceedings of the 9th Congress of Applied Mechanics*, Brussels, p. 245.

Irwin, G. (1960a). *Fracture Mechanics in Structural Mechanics*. Pergamon Press, Oxford.

Irwin, G. (1960b). Plastic zone near a crack and fracture toughness. *Proceedings of the 7th Sagamore Ordnance Materials Conference*, Syracuse University, New York.

Ju, F. and Minovich, M. (1986). Modal frequency method in diagnosis of fracture damage in structures. *Proceedings of the 4th International Modal Analysis Conference*, Los Angeles, CA.

Karaagac, C., Ozturk, H., Sabuncu, M. (2011). Crack effects on the in-plane static and dynamic stabilities of a curved beam with an edge crack. *Journal of Sound and Vibration*, 330(8), 1718–1736.

Khiem, N. and Lien, T. (2001). A simplified method for natural frequency analysis of a multiple cracked beam. *Journal of Sound and Vibration*, 245(4), 737–751.

Kirsch, E. (1898). Die theorie der elastizität und die bedürfnisse der festigkeitslehre. *Zeitschrift des Vereines deutscher Ingenieure*, 42, 797–807.

Kirshmer, P. (1944). The effect of discontinuities on the natural frequency of beams. *Proceedings of ASTM International*, 44, 897–904.

Kisa, M. and Arif Gurel, M. (2007). Free vibration analysis of uniform and stepped cracked beams with circular cross sections. *International Journal of Engineering Science*, 45(2–8), 364–380.

Krawczuk, M., Palacz, M., Ostachowicz, W. (2003). The dynamic analysis of a cracked Timoshenko beam by the spectral element method. *Journal of Sound and Vibration*, 264(5), 1139–1153.

Mazanoglu, K., Yesilyurt, I., Sabuncu, M. (2009). Vibration analysis of multiple-cracked non-uniform beams. *Journal of Sound and Vibration*, 320(4–5), 977–989.

Müller, W., Herrmann, G., Gao, H. (1993). A note on curved cracked beams. *International Journal of Solids and Structures*, 30, 1527–1532.

Orhan, S. (2007). Analysis of free and forced vibration of a cracked cantilever beam. *NDT & E International*, 40(6), 443–450.

Ostachowicz, W. and Krawwczuk, M. (1992). Coupled torsional and bending vibrations of a rotor with an open crack. *Archive of Applied Mechanics*, 62, 191–201.

Pau, A., Greco, A., Vestroni, F. (2010). Numerical and experimental detection of concentrated damage in a parabolic arch by measured frequency variations. *Journal of Vibration and Control*, 17(4), 605–614.

Peano, G. (1888). Intégration par séries des équations différentielles linéaires. *Mathematische Annalen*, 32(3), 450–456.

Pease, M. (1965). *Methods of Matrix Algebra*. Academic Press, New York.

Pestel, E. and Leckie, F. (1963). *Matrix Methods in Elastomechanics*. McGraw-Hill, New York.

Pflüger, A. (1964). *Stabilitätsprobleme der Elastostatik*. Springer-Verlag, Berlin.

Pignataro, M. and Ruta, G. (2003). Coupled instabilities in thin-walled beams: A qualitative approach. *European Journal of Mechanics – A/Solids*, 22(1), 139–149.

Pignataro, M., Rizzi, N., Luongo, A. (1991). *Stability, Bifurcation and Post-critical Behaviour of Elastic Structures*. Elsevier, Amsterdam.

Pignataro, M., Rizzi, N., Ruta, G. (2008). A beam model for the flexural-torsional buckling of thin-walled members. *Thin Walled Structures*, 46, 816–822.

Rice, J. (1968). A path independent integral and the approximate analysis of strain concentration by notches and cracks. *ASME Journal of Applied Mechanics*, 35, 379–386.

Rice, J. and Levy, N. (1972). The part-through surface crack in an elastic plate. *Journal of Applied Mechanics*, 39, 185–194.

Simitses, G. and Hodges, D. (2006). *Fundamentals of Structural Stability*. Butterworth-Heinemann, Burlington.

Sinha, J.K. and Friswell, M.I. (2002). Simulation of the dynamic response of a cracked beam. *Computers and Structures*, 80(18–19), 1473–1476.

Slavik, A. (2007). *Product Integration, its History and Applications*. Matfyz Press, Prague.

Tada, H., Paris, P., Irwin, G. (2000). *The Stress Analysis of Cracks Handbook*, 3rd edition. ASME Press, New York.

Thomson, W. (1949). Vibration of slender bars with discontinuities in stiffness. *Journal of Applied Mechanics*, 17, 203–207.

Timoshenko, S. and Gere, J. (1961). *Theory of Elastic Stability*. McGraw-Hill, New York.

Timoshenko, S. and Goodier, J. (1951). *Theory of Elasticity*, 2nd edition. McGraw Hill, New York.

Tufekci, E. and Arpaci, A. (2006). Analytical solutions of in-plane static problems for non-uniform curved beams including axial and shear deformations. *Structural Engineering and Mechanics*, 22(2), 131–150.

Tufekci, E., Eroglu, U., Aya, S. (2017). A new two-noded curved beam finite element formulation based on exact solution. *Engineering with Computers*, 33(2), 261–273.

Viola, E., Nobile, L., Federici, L. (2002). Formulation of cracked beam element for structural analysis. *Journal of Engineering Mechanics*, 128(2), 220–230.

Wang, C., Wang, C., Reddy, J. (2005). *Exact Solutions for Buckling of Structural Members*. CRC Press, Boca Raton.

Wells, A. (1963). Application of fracture mechanics at and beyond general yielding. *British Welding Journal*, 11, 563–570.